Shear-Induced Structure Formation in MAH-g-PP Compatibilized Polypropylenes

Macromolecules

pubs.acs.org/Macromolecules

Article

Shear-Induced Structure Formation in MAH-g-PP Compatibilized Polypropylenes

Stan F. S. P. Looijmans,* Dario Cavallo, Daniel Hermida Merino, Juan Carlos Martinez, Patrick D. Anderson, and Lambèrt C. A. van Breemen*

Cite This: *Macromolecules* 2023, 56, 5278−5289

Read Online

ACCESS | Metrics & More | Article Recommendations | Supporting Information

ABSTRACT: The effect of maleic-anhydride-grafted polypropylene compatibilizer on the crystallization behavior of two isotactic polypropylene homopolymers is experimentally investigated under both quiescent and shear flow conditions. A traditional combination of optical microscopy and calorimetric techniques is used to quantify crystal nucleation and growth rates and suggests a minute increase in nucleation density when the compatibilizer is added. The flow properties of these systems are assessed by means of oscillatory shear rheometry. The altered flow characteristics can be explained based on the molecular weight distribution of the individual blend components, and no influence of maleic anhydride incorporation on the rheological properties is found. While the addition of a small amount of this compatibilizer thus leads to only a slight acceleration of the crystallization kinetics in quiescent conditions, it markedly enhances the crystallization rate when a mild (and strong) shear flow is applied. In the latter case, the resulting morphology and crystal modification are considerably different as compared to crystallization conditions without the presence of flow; in addition to having significantly faster flow-induced crystallization kinetics (I), when the system contains maleic anhydride compatibilization, the formation of oriented structures is hindered (II), and the appearance of the β-modification is suppressed (III) with respect to the homopolymers, which in turn affects the mechanical properties of the material. This result highlights the importance of understanding the crystallization kinetics under processing relevant conditions in order to get a step closer toward full control over the crystallizing microstructure and the subsequent mechanical performance of polyolefin-based composites.

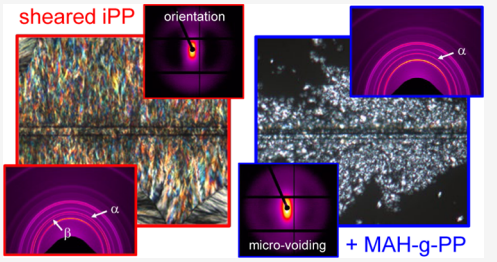

INTRODUCTION

Maleic-anhydride-grafted polypropylenes are widely used to compatibilize glass-fiber-reinforced polypropylene composites[1−4] as well as thermoplastic blends[5−7] and (partially) biobased composites.[6,8−11] With increasing demand for high-end applications and the global strive toward full recyclability of polyolefins, compatibilization of such materials has regained the interest of both academia[12,13] and industry.[14] Although several synthetic functionalization pathways are well-studied,[5,15−24] the subsequent effect on the bulk crystallization of isotactic polypropylene (iPP) is still underexposed; under quiescent conditions, Cho et al. observed a slight increase in the crystallization temperature and thus in the non-isothermal crystallization kinetics above a critical grafting content.[25] However, in particular, under processing relevant conditions, the literature on crystallization and morphology development of compatibilized polypropylene is still void.

Already in the early days of glass-fiber-reinforced polypropylene, it was discovered that a mild nonaffine motion of a fiber with the flow can lead to the formation of α-row nuclei, on which β-phase can form.[26] This phenomenon is well-studied by many authors over the past decades[27−32] for various fiber types[33] but always for moderate to high molecular weight and, most importantly, noncompatibilized polypropylenes. Until now, the possibility of the compatibilizer interfering with the above-described structure formation is never considered, neither on the single-fiber level nor on bulk crystallization. The experimental observation that in fact the addition of an adhesion modifier leads to a substantial change in interphase crystallization around a single fiber is the prime motivation for the present work.

On the other hand, ample investigations into the effectiveness of matrix compatibilization and fiber surface functionalization on the mechanical performance of glass-fiber-reinforced iPP materials have been conducted,[34−37] yet sometimes contradictory results are found; although most authors agree on the improvement of the bond strength between the fiber and matrix when the interface is comprised of a so-called transcrystalline or columnar layer,[38−41] specifically when this layer consists of the tough β-modification,[42,43] exemptions can be found.[44,45] Given the

Received: April 3, 2023
Revised: June 27, 2023
Published: July 13, 2023

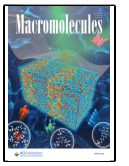

lack of a universal testing method for determining the interfacial strength in fiber-reinforced polymer composites,[4,38,44−47] the inherent complexity of the multiphase, multimorphology crystallization of iPP under practical processing conditions,[48] and the wide variety of chemistries and material formulations used,[36,39,42−45,49] the identification of the exact role of each parameter is proven to be a delicate task.

Under quiescent and moderate cooling conditions, highly isotactic polypropylenes typically crystallize into a spherulitic morphology composed of radially outward growing bundles of α-phase lamellae.[50] When the cooling rate is sufficiently large, i.e., around 100 K/s, a nodular structure of mesophase is formed,[51] while at elevated pressures the γ-phase is predominant.[52,53] Under special conditions and in a relatively narrow temperature window, the β-phase of iPP can form,[54,55] usually most pronounced upon a combination of a mild temperature gradient[56,57] and flow.[58,59] Although this phase is only metastable from a thermodynamic point of view, its transition into the stable α-form is so slow that it remains in this form almost indefinitely. The β-modification possesses superior mechanical performance, showing slightly lower yet comparable yield stress with respect to the α-phase, and yet significantly larger ductility and lifetime.[60] Therefore, to promote the formation of the β-phase, often a selective nucleating agent is added,[61] yet from a recyclability perspective, nowadays this practice may be undesirable.

To systematically investigate the effect of (MAH-g-PP) matrix compatibilization in fiber-reinforced polypropylene composites, the crystallization kinetics (I), morphological superstructure (II), and phase composition (III) of the bulk polymer matrix are assessed while mimicking relevant industrial-scale processing conditions, i.e., high pressures, shear rates, and temperature gradients. By leaving the fiber-reinforcement out, the influence of the variation in local stiffness, differences in thermal expansion, and the nonaffine motion between fiber and matrix is unambiguously excluded. While (in line with earlier findings[25]) the quiescent crystallization kinetics and linear rheology appear to be only marginally affected by the addition of a realistic amount (up to 5%) of MAH-g-PP compatibilizer, as soon as a shear flow is applied, the effects are remarkable; in the compatibilized blend, under the exact same flow conditions, (I) the crystallization kinetics may be accelerated by a factor of 10, (II) the morphological superstructure changes from an oriented, shish−kebab type of structure to a microspherulitic one, and (III) the phase composition changes from predominantly β-phase in a neat iPP sample to solely α-phase when MAH-g-PP is added. These findings demonstrate that MAH-g-PP, apart from enhancing the adhesion between the fiber and matrix, completely changes the crystallization behavior of the matrix. Moreover, due to the exclusion of the fiber reinforcement, it is proven that this effect is related to the bulk matrix and not determined by any type of interaction between the fiber and matrix. In a way, the addition of MAH-g-PP compatibilizer acts as a flow-activated nucleating agent for the α-phase of polypropylene, which could potentially be utilized in applications where optical appearance is of importance.

EXPERIMENTAL METHODS

Materials and Sample Preparation. Two commercially available homopolymer grades of isotactic polypropylene (iPP) are kindly provided by Borealis Polyolefine GmbH (Linz, Austria). The sample referred to as iPP-1 is a material optimized for composite production and has a weight-average molecular weight of 130 kg/mol and a polydispersity index of 5.5. As a reference material, an extensively studied injection molding grade, HD601CF, with a weight-average molecular weight of 365 kg/mol and a polydispersity of 5.5 (iPP-2), is used.[62,63] Both materials are based on the same post-phthalate Ziegler−Natta catalyst system and have the same degree of isotacticity. To study the effect of MAH-g-PP compatibilizer on the crystallization kinetics of iPP, a commercially available masterbatch (Exxon PO1020) with high grafting content, i.e., classified as a MAH content between 0.5 and 1 wt %, is mixed into both previously mentioned homopolymers. Two industrially relevant blend compositions of 2.5 and 5 wt % MAH-g-PP are compounded using a ThermoElectron Rheomex OS-PTW 16 twin-screw extruder (kindly provided by PTG/e) with corotating screws of L/D = 40. The monofilament is quenched and subsequently pelletized to make it suitable for further sample preparation. For all materials described above, the complete molar mass distribution, and in the case of MAH-g-PP, the composition distribution are provided in the Supplementary Material.

Thermal Analysis. The crystallization kinetics of the supercooled melt under quiescent conditions are determined for isothermal and non-isothermal histories by means of differential scanning calorimetry (DSC). Samples of ≈4 mg are placed in 40 μL aluminum crucibles and loaded into the autosampler of a Mettler−Toledo DSC 823e equipped with a Cryostat intracooler for controlled cooling rates up to 20 K/min. The sample is heated to 200 °C at a rate of 20 K/min and kept for 5 min to remove its thermomechanical history. This temperature and isothermal time are determined to be sufficient based on the rheological relaxation times and melt-memory analysis measured by DSC. Subsequently, the sample is cooled at a rate of 20 K/min to room temperature (for the non-isothermal experiments) or to the desired isothermal crystallization temperature. Temperature, melting enthalpy, and thermal lag have been calibrated using indium and zinc calibration standards. The furnace is continuously purged with a nitrogen flow of 50 mL/min. To extend the temperature range to practically relevant processing temperatures, isothermal crystallization experiments are performed in the range of 0−100 °C on a Mettler−Toledo Flash DSC (FDSC), equipped with a Huber TC100 intracooler. Using a sample mass in the order of nanograms melted onto a UFS-1 sensor, heating rates up to 50,000 K/s and cooling rates up to 5000 K/s are achieved, which allow to capture the isothermal crystallization kinetics of iPP down to its glass transition temperature. Samples are heated to 200 °C at a rate of 5000 K/s and after a hold time of 1 s, cooled to the selected crystallization temperature at 5000 K/s. Prior to the sample preparation, the UFS-1 sensor is conditioned five times and corrected according to the specifications of the manufacturer. During the experiment, a continuous nitrogen flow of 20 mL/min is applied.

The crystallization process of iPP can be split into two mechanisms, i.e., nucleation and growth. Using the calorimetric techniques described above, mostly a combination of these two processes is measured, although certain ad hoc protocols to split the two exist.[64] A better-defined method however, is the quantification of crystal growth rates by means of polarized optical microscopy (POM). In such experiments, the time evolution of the radius of individual spherulites is extracted from an image series or video. Polymer particles are heated to 230 °C on a hot plate and subsequently compressed between two microscope glass slides until a film thickness of ≈20 to 40 μm is achieved. These films are then reheated in a Linkam TS350 heating stage with a TP93 temperature controller. Temperature and thermal lag due to the presence of the glass slides are calibrated and corrected for. Images are acquired using an Olympus Colorview III digital camera mounted on an Olympus BX51 microscope operated in transmission mode at a magnification of 20×. Radial growth rates are determined from the linear slope of the radius versus time curves.

Using the above-described sample preparation method, four different single-fiber composite samples are prepared. The thin polymer films are remolten around a commercially available continuous, silane-sized glass fiber, optimized for compatibilized

https://doi.org/10.1021/acs.macromol.3c00603
Macromolecules 2023, 56, 5278−5289

polyolefin impregnation, with a diameter of 17 μm (Nippon Electric Glass, Otsu, Japan) at a temperature of 200 °C, equilibrated for 5 min, and subsequently cooled to the isothermal crystallization temperature of 130 °C. For the sheared samples, the fiber is displaced over a distance of 1 mm in 1 s as soon as the temperature reaches the isothermal crystallization temperature. Additional details on the sample preparation method can be found in our previous work.[33]

Gel Permeation Chromatography. All parameters of the molecular weight distribution (MWD) were determined by gel permeation chromatography (GPC) according to ISO 16014-4:2003. A PolymerChar GPC instrument, equipped with an infrared (IR) detector was used with 3× Olexis and 1× Olexis Guard columns from Polymer Laboratories and 1,2,4-trichlorobenzene (TCB, stabilized with 250 mg/L 2,6-di-*tert*-butyl-4-methyl-phenol) as the solvent at 160 °C and at a constant flow rate of 1 ml/min. 200 μL of the sample solution was injected per analysis. The column set was calibrated using universal calibration (according to ISO 16014-2:2003) with at least 15 narrow MWD polystyrene (PS) standards in the range of 0.5−11 500 kg/mol. Mark Houwink constants used for PS, PE, and PP are as described per ASTM D 6474-99. All samples were prepared by dissolving 5.0−9.0 mg of polymer in 8 mL (at 160 °C) of stabilized TCB (same as mobile phase) for 2.5 h at 160 °C under continuous gentle shaking in the autosampler of the GPC instrument.

To characterize the maleic anhydride distribution over the molecular weight distribution of the compatibilizer, GPC-IR6 measurements are performed using a PolymerChar 2D-LC high-temperature chromatograph (Valencia, Spain). The instrument is used in GPC mode, bypassing the HPLC column. The instrument is equipped with a PLgel Olexis GPC column (300 × 7.5 mm L × I.D., 13 μm particle size). A sample loop of 100 μL inner volume was applied. The measurements were performed at 140 °C. Detection was realized with a fixed wavelength infrared (IR) detector (IR6, PolymerChar), with detection capabilities (bandpass filters) for overall polymer concentration, CH_2, CH_3, and C═O. GPC elution times are calibrated with polystyrene (EasiCal PS-1, Agilent, Waldbronn, Germany). The mobile phase was 1,2-dichlorobenzene (ODCB, Acros Organics, Schwerte, Germany). The mobile phase flow rate was 1 mL/min. Sample concentrations were ≈5 g/L, 6 mL of the mobile phase was automatically added to the sample vials (containing weighed polymer) by the autosampler, while simultaneously flushing them with nitrogen. The sample was dissolved, under shaking, for 1 h prior to injection. The sample is independently prepared and analyzed two times.

Rheometry. The effect of MAH-g-PP addition on the flow behavior of iPP is characterized on a MCR 502 rheometer (Anton Paar, Graz, Austria) equipped with a convection oven. A parallel-plate geometry with a plate diameter of 25 mm was used at a gap of ≈1 mm. A strain sweep at a frequency of 1 rad/s is performed at the lowest (145 °C) and highest (265 °C) testing temperatures. The sample is always molten at 265 °C for 5 min before being cooled at 10 K/min to the test temperature. At test temperatures below the melting point of the polymer, the measurement time is kept sufficiently short to prevent the onset of crystallization. A strain of 1% is selected as optimum since it is well within the linear regime of the materials yet still provides sufficient torque resolution at higher temperatures. Using this strain, small-amplitude oscillatory shear (SAOS) frequency sweeps are measured from 0.1 rad/s to 100 rad/s at 15 °C temperature intervals between 145 and 265 °C. Although the convection oven is continuously flushed with nitrogen, for each testing temperature, a new sample is used to prevent thermal degradation. Samples are prepared by compression molding 25 mm diameter disks of 1 mm thickness on a Fontijne Holland (TP 400) compression molding machine. Pellets are sandwiched between PTFE sheets to prevent adhesion to the mold and heated to 230 °C in the hot section of the press. After 10 min of melting, a force of 100 kN is applied and held constant for 3 min. Subsequently, the stack is placed in the cold section of the press, where water-cooled plates kept at 20 °C extract heat from the sample.

Extended Dilatometry. The specific volume of various iPP grades is characterized using a Pirouette dilatometer (IME Technologies, Eindhoven, The Netherlands).[65,66] This device allows to measure the volume of a material as a function of pressure and temperature, similar to standard PVT techniques, but in addition is capable of performing these measurements under non-isothermal and shear flow conditions. First, a ring-shaped sample is injection molded using a Babyplast (Rambaldi, Italy) lab-scale device equipped with a custom-designed mold. These rings, with a height of 2.5 mm, an outer diameter of 22 mm, and a thickness of 0.5 mm, have a resulting weight of solely ≈70 mg. The exact dimensions are measured using a Mitutoyo micrometer with a resolution of 1 μm and the weight of the individual rings is determined using a Mettler−Toledo XS105DU balance (Columbus, Ohio). The ring is then sealed between two PTFE rings of similar size and placed over the rotor of the PVT device. After the stator is placed on top, the temperature is increased to 230 °C and held for 10 min to eliminate its thermomechanical history. Then, a pressure of 100, 300, 600, or 900 bar is applied and held constant, after which the sample is cooled to room temperature at an average rate of 1 K/s in the crystallization window. During cooling, a shear pulse of 1 s is applied at temperatures corresponding to 130 and 150 °C at atmospheric pressure, i.e., at undercoolings[67,68] of 60 and 40 °C, while the sample height is recorded as a function of temperature. Due to the confinement of the sample between the rotor and the stator, the sample height is easily converted into a specific volume. From the specific volume versus temperature curve, the onset of crystallization temperature is determined. Analogous to previous work done in our group,[68] the crystallization temperature is normalized according to

$$T_\theta = \frac{T_{\text{onset},\dot\gamma}}{T_{\text{onset},q}} \tag{1}$$

where $T_{\text{onset},\dot\gamma}$ and $T_{\text{onset},q}$ are evidently the crystallization onset temperatures in Kelvin in shear and quiescent conditions.

The parameter that is used to describe the strength of the flow in these experiments is the temperature- and pressure-dependent Weissenberg number given by

$$Wi = a_p a_T \tau_R \dot\gamma \tag{2}$$

in which $\dot\gamma$ is the applied shear rate, a_p and a_T the pressure and temperature shift factors, respectively, τ_R the governing relaxation time of the high-molecular-weight tail with its reference at 190 °C and atmospheric pressure. The determination of this parameter is described in full detail in the Supplementary Material. The temperature shift is described by the WLF relation

$$\log(a_T) = \frac{-c_1(T - T_{\text{ref}})}{c_2 + (T - T_{\text{ref}})} \tag{3}$$

where c_1 and c_2 are fit parameters of the linear rheological data, T the absolute temperature, and T_{ref} the reference temperature of 463 K. The pressure shift factor is determined according to[69]

$$a_p = \exp(\kappa(p - p_0)) \tag{4}$$

with κ the pressure dependency taken from ref 70, p the absolute pressure, and p_0 the (reference) atmospheric pressure of 1 bar. The relevant parameters in the above equations are provided in Table S1.

Structure Quantification. Two sets of synchrotron X-ray experiments are performed. A combined small-angle scattering and wide-angle diffraction (SAXS/WAXD) setup at the BL11 NCD-SWEET beamline of the ALBA synchrotron (Barcelona, Spain)[71] is used to quantify the microstructure of the samples prepared in the dilatometer. A Pilatus 1 M area detector (Dectris, Baden, Switzerland) with a pixel size of 172 × 172 μm^2 is used to collect high-resolution SAXS images at a distance of 6.24 m from the sample, while quasi-2D WAXD patterns are acquired using an LX255-HS area detector (Rayonix, Evanston Illinois) placed at a distance of 169 mm, having a tilt angle of 30° with respect to the chain-orientation direction within the sample. The pixel size of this detector is 44.3 × 44.3 μm^2, yet in this experiment, the device is utilized in 2 × 2 binning mode. The beamline is operated at a photon energy of 12.4 keV, corresponding

https://doi.org/10.1021/acs.macromol.3c00603
Macromolecules 2023, 56, 5278−5289

to a wavelength λ = 0.999 Å. The geometry is calibrated using silver behenate (AgBh) for the small angles and chromium(III)oxide (Cr_2O_3) for the wide angles. Samples are mounted on an aluminum multisample holder with 4 mm holes using a double-sided adhesive tape.

The in situ crystallization kinetics in both quiescent and shear conditions are determined using a combined SAXS/WAXD setup at the BM26 DUBBLE beamline, part of the European Synchrotron Radiation Facility (ESRF) Grenoble, France.[72] Similar to the previously described configuration, a Pilatus 1 M area detector is used to acquire 2D SAXS patterns at a distance of 3.44 m. In this case, WAXD images are captured on a Pilatus 300K photon-count detector with a pixel size of 172 × 172 μm^2 that is mounted at a distance of 302 mm from the sample at a tilt angle of 8°. During this experiment, the BM26 beamline is operated at a photon energy of 12 keV, which corresponds to an X-ray wavelength of λ = 1.033 Å. Calibration of the scattering geometry is done using silver behenate (SAXS) and aluminum oxide (WAXD). Two different sample environments are used: a Linkam DSC 600 heating cell to perform isothermal crystallization experiments and a Linkam CSS450 shear cell to study shear-induced structure formation in a parallel-plate geometry. Analogous to the above-described DSC experiments, the 2 mg sample is molten at 230 °C to erase the thermomechanical history and to assure proper contact with the aluminum pan (TA instruments, 20 μL) and subsequently cooled at a rate of 20 K/min to the desired isothermal crystallization temperature (125, 130, and 135 °C, respectively) after which the structure formation is followed in time until full space-filling is reached. The exact same temperature protocol has been applied to 25 mm diameter disk-shaped samples (thickness of ≈1 mm) that are placed in the shear cell and slightly compressed between the two X-ray transparent windows (polyimide and diamond). At an isothermal crystallization temperature of 133 °C, a shear pulse of 1 s at rates of 10, 50, and 90 s^{-1} is applied and the structure formation is followed for 30 min.

For all X-ray scattering/diffraction measurements, the acquired patterns are normalized to the incident beam intensity and background-subtracted. Data integration is done using the FIT2D open-source software developed by the ESRF.[73−75] The crystallinity is determined by fitting an amorphous halo obtained from an atactic polypropylene sample to the noncrystalline regions of the diffraction pattern, i.e., the region at low and high q where no diffraction peaks are visible. The area A_{total} beneath the diffraction pattern and A_{amorph} below the fitted amorphous halo, as indicated in Figure 1, are used to calculate the weight fraction crystallinity

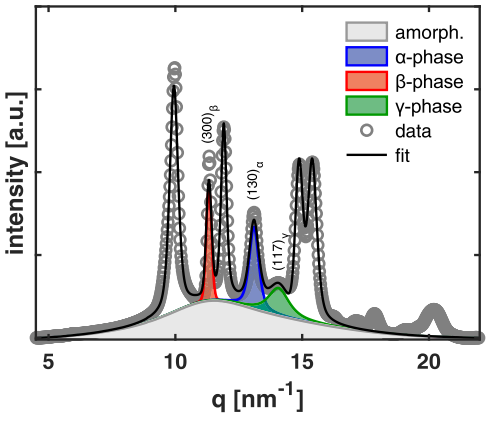

Figure 1. Example of a normalized, integrated WAXD pattern of a semicrystalline, isotactic polypropylene sample that contains α, β, and γ-phases. The amorphous halo is fitted first; thereafter, the crystalline peaks are deconvoluted. The relevant deconvoluted diffraction peaks of the individual phases are indexed and colored.

$$\chi = \frac{A_{total} - A_{amorph}}{A_{total}} \tag{5}$$

Subsequently, the crystalline diffraction peaks are deconvoluted using Voigt functions to obtain the respective intensities from which the phase composition is then calculated. Because of significant overlap between the diffraction peaks of the α- and γ-phases of polypropylene, the integrated intensity below $(130)_\alpha$, $(300)_\beta$, and $(117)_\gamma$ is used to calculate the relative fraction of phase i = α, β, γ according to[60,76]

$$\chi_i = \frac{A_i}{A_{(130)_\alpha} + A_{(300)_\beta} + A_{(117)_\gamma}} \tag{6}$$

The average lamellar thickness of these crystals is calculated from the 1D Lorenz-corrected SAXS data. First, the 2D scattering data is azimuthally integrated, i.e., integrated over the angle ϕ as schematically depicted in the left panel of Figure 2a, and plotting the obtained intensity versus the scattering vector q

$$q = \frac{4\pi}{\lambda}\sin(\theta) \tag{7}$$

in which λ is the wavelength of the incident light (X-rays in this case) and θ is half of the scattering angle. For an isotropic scattering system, the long period is determined from the Iq^2 versus q plot, as indicated in Figure 2b, according to

$$L_p = \frac{2\pi}{q_{max}} \tag{8}$$

where q_{max} is the absolute value of the scattering vector at the point where Iq^2 is maximum. When multiplied by the density-corrected crystallinity χ_V, the lamellar thickness is obtained

$$L_c = \chi_v \cdot L_p = \frac{(\chi/\rho_c)}{(\chi/\rho_c) + ((1-\chi)/\rho_a)} \cdot L_p \tag{9}$$

where ρ_c and ρ_a refer to the density of crystalline (946 kg/m^3) and amorphous phases (850 kg/m^3) at room temperature, respectively.[76−78]

RESULTS AND DISCUSSION

As stated before, the prime motivation for this research is the strongly altered interphase morphology around a glass fiber subjected to shear flow when a matrix compatibilizer MAH-g-PP is added to a neat iPP matrix. While studying the formation of transcrystallinity around a glass fiber,[33] under quiescent conditions, the addition of 5% MAH-g-PP compatibilizer appears to have a minute effect on the microstructure that develops, as presented in the polarized optical micrographs of the central panel of Figure 3 and in line with earlier observations.[25] However, when performing a fiber-pulling experiment to induce a clear transcrystalline layer, a remarkable difference between the structure formed in the compatibilized matrix with respect to the nonmodified matrix is found; rather than developing a columnar layer of oriented β-phase crystals (top right panel), a large number of small, spherical α-phase spherulites form (bottom right panel). Even though it is highly unlikely that this phenomenon has not been observed before, the authors are not aware of any literature discussing this matter. At first consideration, one might argue that due to an improved chemical interaction between the fiber and the matrix, the local mobility of the polymer chains is restrained, which might enhance the local nucleation efficiency. However, given the considerable distance from the fiber where the nucleation density is still strongly enhanced (≈100 to 200 μm), this hypothesis is deemed improbable. Instead, it is hypothesized that the observation is a bulk matrix effect and

https://doi.org/10.1021/acs.macromol.3c00603
Macromolecules 2023, 56, 5278−5289

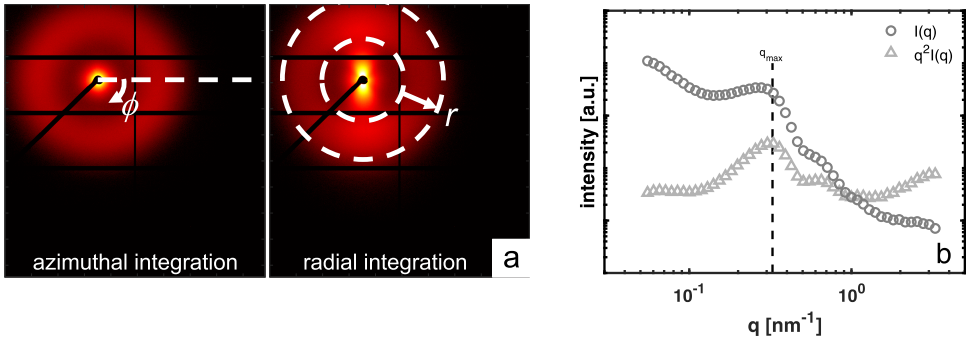

Figure 2. (a) Example of an isotropic (left) and anisotropic (right) iPP sample with most relevant integration principles indicated. (b) Example of a normalized, azimuthally integrated SAXS pattern of a semicrystalline, isotactic polypropylene sample. The Lorenz-corrected 1D data $q^2I(q)$ is used to determine q_{max}, i.e., the magnitude of the scattering vector at maximum 1D intensity, from which the average long spacing can be calculated.

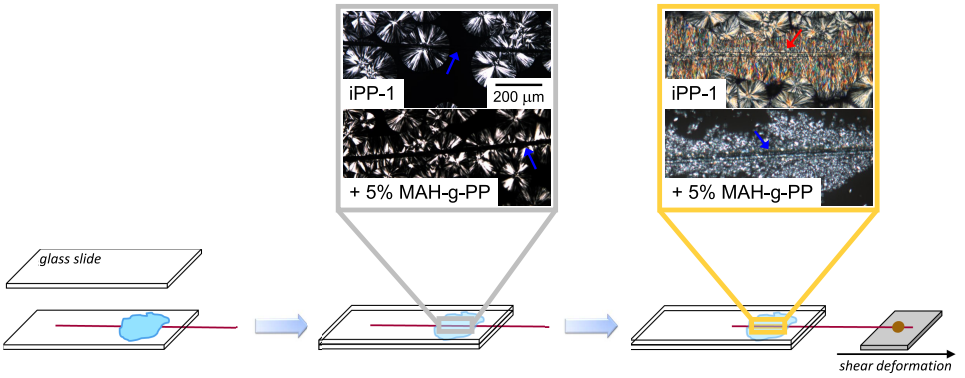

Figure 3. Example of the typical microstructures observed at the interphase in a fiber-reinforced iPP composite material after the addition of MAH-g-PP compatibilizer. The structure formation under quiescent conditions is presented in the central panel, whereas the right panel displays the crystallizing microstructure after a 1 s shear pulse of 1 mm/s to the fiber. The location of the fiber (aligned in the horizontal plane) is indicated by the arrows.

becomes only apparent at the interphase because of the locally applied shear flow. Therefore, a fiber-free matrix system under various processing conditions is considered. Note that neither during the melting at elevated temperatures nor upon cooling and subsequent isothermal crystallization, inhomogeneities in the undercooled melt are observed. Hence, the concentration of MAH in the MAH-g-PP/iPP blend is considered to be sufficiently low to inhibit macroscopic phase separation, a phenomenon commonly observed when the concentration of MAH-g-PP is above a critical value.[79] Due to the extreme low concentration of functional groups in the blended system, the role of potential shear-induced phase separation at the nanoscale in the increased nucleation density at the interphase can solely be speculative as experimental verification is challenging.

In order to systematically quantify the influence of MAH-g-PP on the crystallization behavior of polypropylene, first isothermal and quiescent conditions are considered. Under these conditions, the process is typically well described by an undercooling-dependent nucleation density $N(T)$ and crystal growth rate $G(T)$.[80] In the past, numerous crystallization models for iPP have been developed,[48,81−86] all with similar characteristics. At low supercooling, the nucleation process is dominated by the presence of foreign substances, i.e., fibers, particulate fillers such as colorants, nucleating agents, or other impurities, which may reduce the energy barrier for nucleation. On the other hand, at high undercooling, the nucleation process is governed by the spontaneous arrangement of chain segments due to thermal fluctuations that become stable due to the large difference between the crystallization temperature and melting temperature.

Using a combination of differential scanning calorimetry (DSC) and polarized optical microscopy (POM), the effect of MAH-g-PP compatibilization on the crystallization kinetics of iPP is analyzed; the crystallization halftime as a function of temperature is presented in Figure 4a, where irrespective of the sample, clearly, the homogeneous and heterogeneous nucleation-dominated regimes can be distinguished. The crystal growth rates shown in Figure 4b are obtained by tracking spherulite radii in time at a constant temperature. The radial growth rates of iPP-1, iPP-2, and MAH-g-PP as well as the compatibilized blends are found to be identical and comparable to literature results on which the model prediction (drawn curve) is found.[80] The crystallization halftime (Figure 4a), being a measure of the overall kinetics, is significantly lower when 5% MAH-g-PP is added to the iPP matrix material compared to the individual constituents, yet solely in the heterogeneous nucleation regime and particularly in the temperature window that is practically relevant, i.e., between 50 and 100 °C. It should be noted that, in order to make a fair comparison, the neat iPP-1 material has the exact same thermomechanical history; it is run through the twin-screw compounder, quenched, and repelletized analogous to the blends. The addition to MAH-g-PP thus leads to a decrease in crystallization halftime, i.e., an increase in overall crystallization kinetics, while it does not at all affect the spherulitic growth

https://doi.org/10.1021/acs.macromol.3c00603
Macromolecules 2023, 56, 5278−5289

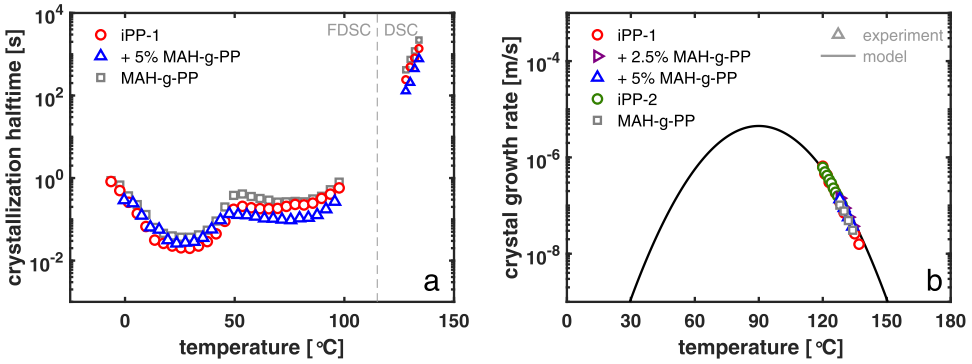

Figure 4. (a) Influence of MAH-g-PP on the crystallization halftime of iPP after isothermal crystallization at the indicated temperatures. An acceleration of the crystallization kinetics is observed solely in the heterogeneous nucleation regime. (b) Crystal growth rate as a function of isothermal crystallization temperature determined by POM. The lamellar growth rate is not affected by the presence of a compatibilizer.

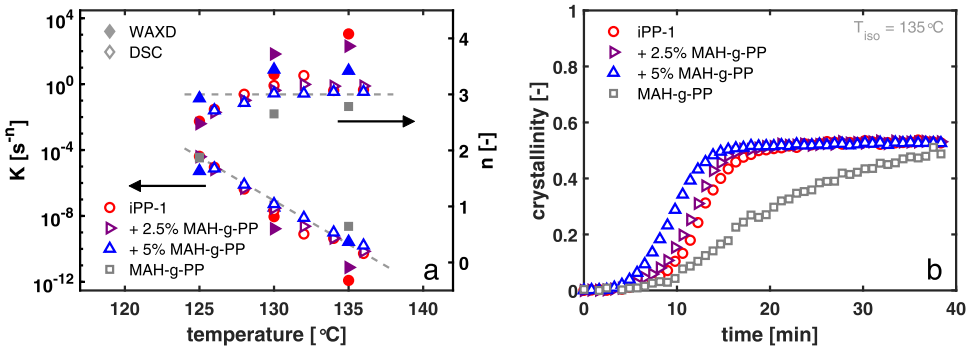

Figure 5. (a) Avrami parameters of crystallization as measured by DSC and in situ WAXD. (b) Crystallinity evolution upon quiescent, isothermal crystallization at 135 °C determined by in situ WAXD analysis.

rate. This suggests that the compatibilization lowers the free-energy barrier for nucleation, therewith increasing the nucleation density in the heterogeneous nucleation regime. These findings are in line with literature reports of Cho et al.[25] who analyzed the crystallization kinetics of MAH-modified iPP for varying grafting densities and found a significant increase in the crystallization temperature during cooling in the DSC, mainly for low concentrations of compatibilizer, similar to our system.

From the isothermal crystallization experiments performed in conventional DSC, at temperatures ranging from 126 to 136 °C, the Avrami parameters that describe the kinetics are shown in Figure 5a. The determination of these values[87,88] along with the experimental data is provided in the Supplementary Material. For the neat iPP-1, iPP-1 with 2.5% and 5% MAH-g-PP compatibilizer added, the Avrami exponent n is found to be identical and close to 3. This suggests that for all of the materials used in this study, under quiescent conditions, the dominant crystallization mechanism is the three-dimensional growth of preexisting nuclei and that with the addition of MAH-g-PP, the initial number of these nuclei increases, given that the spherulitic growth rate is identical (Figure 4b) for all materials considered here. As the bulk nucleation density in the pure MAH-g-PP sample is considerably lower than in the bulk iPP-1 sample, and both are lower than those of the blends, it is hypothesized that the addition of MAH-g-PP lowers the free-energy barrier for nucleation of the abundantly available heterogeneous nuclei in the iPP-1 (and similarly iPP-2) material.

To verify these results, obtain a more reliable crystallinity measure, and deduce the phase composition in these samples, in situ isothermal crystallization experiments have been performed in front of a synchrotron light source. Combined WAXD/SAXS images are recorded as a time series at the DUBBLE BM26B beamline, part of the European Synchrotron Radiation Facility (ESRF) in Grenoble, France.[72] The crystallization temperatures are set to 125, 130, and 135 °C. In Figure 5b, the time evolution of the density-corrected crystallinity is presented for an isothermal temperature of 135 °C. The lamellar thickness can be calculated by eq 9 from the long period, measured from the collected SAXS data after complete space-filling, and is found to be equal for all sample compositions, i.e., is solely a function of crystallization temperature. Lamellar thicknesses are determined to be 9.7, 10.2, and 10.7 nm for all samples crystallized at 125, 130, and 135 °C, respectively. The Avrami parameters calculated from the crystallinity evolution (presented in Figure 5a) are in line with those deduced from DSC and the results presented in Figure 5b confirm the slight acceleration of the crystallization kinetics, while the crystallizing polymorph is always α-phase, the final lamellar thickness is equal for all systems (as is to be expected since the crystallization is isothermal), and the final morphology is in all cases spherulitic, i.e., no lamellar orientation is observed from the SAXS patterns, which is in line with POM observations of the single-fiber composites presented in Figure 3.

The second essential element to understand the behavior of these modified polypropylenes during processing is their response to flow. Small-amplitude oscillatory shear (SAOS) rheology is performed to determine the dynamic moduli and from that the complex viscosity. Frequency sweep tests are performed at constant temperature over the range of 145−265

https://doi.org/10.1021/acs.macromol.3c00603
Macromolecules 2023, 56, 5278−5289

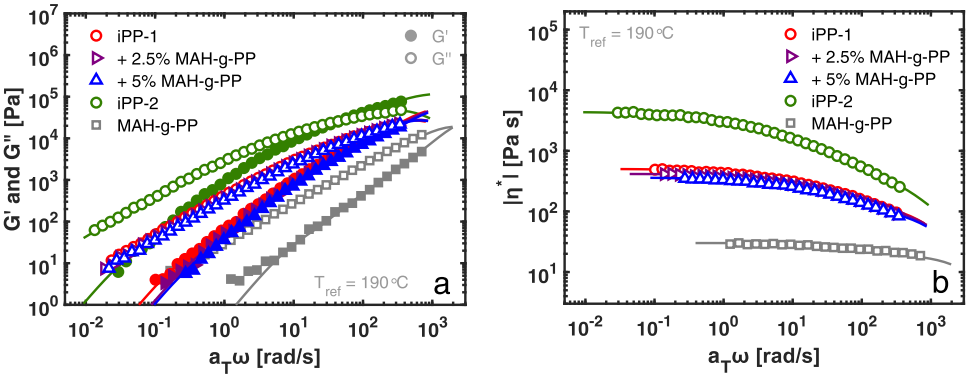

Figure 6. (a) Dynamic moduli of various compatibilized systems measured by SAOS. The addition of MAH-g-PP has a minor influence on the storage and loss moduli. (b) Complex viscosity calculated from the dynamic moduli presented in panel (a).

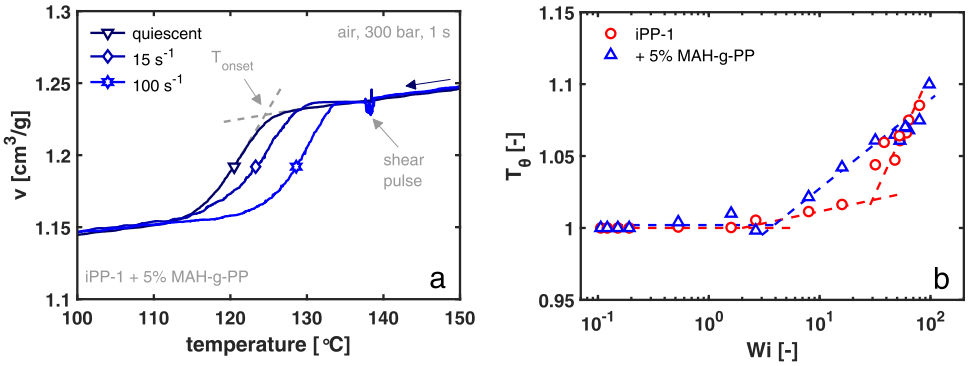

Figure 7. (a) Example of extended dilatometry curves of a MAH-g-PP compatibilized iPP sample measured at 300 bar under air-cooling conditions. (b) Normalized crystallization temperature, i.e., the ratio of the onset temperature under shear flow conditions with respect to its quiescent counterpart as indicated in panel (a) as a function of the flow strength.

°C and shifted to create a mastercurve at 190 °C using the time−temperature superposition principle. The corresponding shift factors are provided in the Supplementary Material and fitted using the Williams−Landel−Ferry (WLF) equation. The representative discrete relaxation time spectrum is determined from a least-square fitting procedure of the multimode Maxwell model to the dynamic moduli, which are presented in Figure 6a where the markers represent the experimental data, while the drawn lines are the model fits. The effect of adding MAH-g-PP to the neat iPP-1 material on its flow properties is best derived from the complex viscosity, which is presented in Figure 6b; at low deformation rates, due to the addition of the low-molecular-weight component, a minor decrease in the zero-shear viscosity is observed, which follows a simple linear rule of mixing. These results are in line with the almost negligible differences in the molar mass distribution that are measured using high-temperature GPC and presented in the Supplementary Material. At increasing deformation rate, i.e., when the material response becomes more elastic, the influence of the added MAH-g-PP to the neat polypropylene vanishes and the dynamic moduli are equal irrespective of the blend composition.

The combination of marginally accelerated crystallization kinetics and a negligible alteration of the flow characteristics of the material does not explain the altered interphase structure observed by POM on the single-fiber composites, in fact, it suggests that under processing conditions, the compatibilized system will exhibit a similar crystallization behavior in terms of rate, phase, and morphology as compared to the neat matrix material. To verify this, extended dilatometry experiments have been performed at a wide range of shear rates, pressures, and supercooling. Sample rings are placed in a confined geometry between two PTFE sealings and heated to 230 °C for 10 min to erase any thermomechanical history from the injection molding step. After the application of an isobaric pressure in the range of 100−900 bar, the sample is cooled at an average rate of ≈1 K/s, while the sample height is recorded as a function of temperature. As the sample geometry is confined in the radial direction, the specific volume can be directly calculated from the sample height. An example of such measurement is presented in Figure 7a. In addition to the application of pressure, a shear pulse of variable duration and rate can be applied to the sample when it reaches a certain temperature. In this work that pulse is always applied for 1 s, which implies that depending on the shear rate the total displacement varies. The shear rates were varied over a wide range from 0 to 180 s^{-1}, which resembles industrially relevant injection molding conditions. Typically, for polyolefins, three regimes can be distinguished depending on the flow strength;[68] at low Weissenberg numbers there is no effect of the applied flow (Regime I), at intermediate Weissenberg numbers (Regime II) the flow creates precursors for crystallization, i.e., flow-enhanced nucleation, and at high Weissenberg numbers the flow is able to crystallize strongly oriented structures often referred to as shish−kebab structures (Regime III). For the neat polypropylenes, all three of these regimes are observed as shown in Figure 7b for iPP-1 and previously reported for iPP-2.[68] When the MAH-g-PP compatibilizer is added, the crystallization temperature in Regime II is substantially increased, which indicates faster crystallization

https://doi.org/10.1021/acs.macromol.3c00603
Macromolecules 2023, 56, 5278−5289

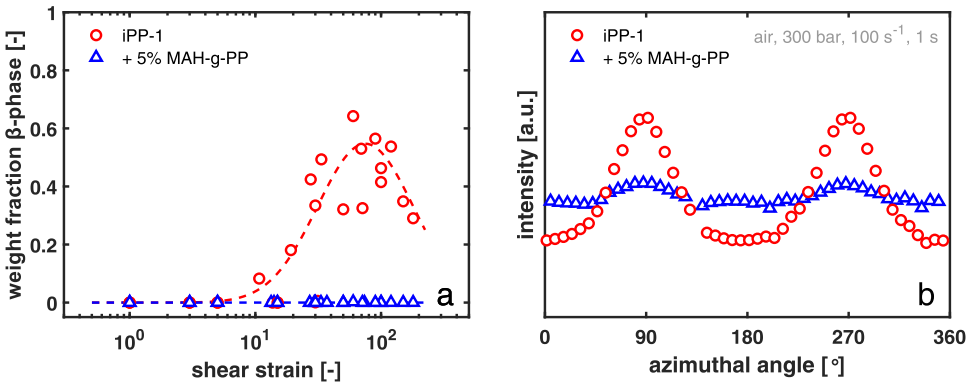

Figure 8. (a) β-phase content determined by post-mortem X-ray analysis of PVT samples. Irrespective of the shear temperature, time, and rate, in the presence of MAH-g-PP, no trace of this crystal modification is found. (b) SAXS intensity as a function of the azimuthal angle for a neat and compatibilized sample crystallized under a strong shear flow.

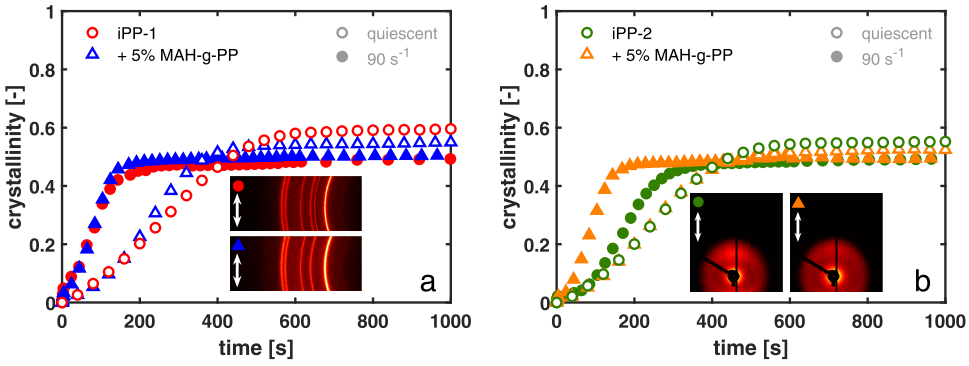

Figure 9. Crystallinity evolution measured by in situ WAXD experiments upon isothermal crystallization in a shear cell at 133 °C and the indicated shear conditions for (a) iPP-1 and (b) iPP-2, together with characteristic 2D WAXD and SAXS patterns upon shear flow, respectively. The arrows indicate the shear direction.

kinetics and a stronger effect of the flow as compared to the neat iPP-1 material. As the crystallization kinetics generally show an exponential dependency with the temperature, the observed increase in crystallization temperature of ≈5−10 °C indicates a 10−1000 times faster crystallization, an effect that is marginally observed in quiescent conditions but strongly enhanced by the application of mild shear flow. Moreover, within the experimental conditions that can be applied by the PVT device, there is no signature of a third flow-induced crystallization (FIC) regime, which suggests that due to the vast number of nuclei that develop, full space-filling is reached before molecular stretch can lead to the formation of oriented structures, a hypothesis that is confirmed by both ex situ and in situ WAXD/SAXS experiments.

Post-mortem X-ray analysis of the PVT sample rings is conducted at the NCD-SWEET BL11 beamline, part of the ALBA synchrotron facility in Barcelona, Spain.[71] Two-dimensional wide- and small-angle X-ray patterns are acquired. The phase composition of the samples is analyzed as described before and the resulting β-phase fraction is presented in Figure 8a. For the neat iPP sample, the fraction of β-modification may be significant; after the application of mild shear, the β-phase reaches up to 60% of the total crystalline fraction. Upon increasing the shear strain, the rapid crystallization of oriented α-phase structures leads to complete space-filling, inhibiting the β-lamellae to grow and as a result, a decrease of β-phase content may be observed in Regime III. A similar, yet more pronounced inhibition of this commonly desired crystal modification is observed in Regime II crystallization of the compatibilized iPP material. Here, solely an α-phase is observed, independent of the applied shear conditions. Upon the application of shear flow, the nucleation efficiency of the MAH-g-PP modified material is strongly enhanced as described before. Due to the rapid space-filling, the formation and growth of highly oriented structures are inhibited, and as a result, a quasi-isotropic morphology develops; the integrated SAXS intensity as a function of the azimuth in Figure 8b demonstrates that while the neat iPP sample exhibits a strong lamellar alignment attributed to the formation of daughter lamellae on the oriented shish,[48,68] the morphology of the compatibilized blend is almost purely isotropic.

In addition to the ex situ X-ray characterization carried out on the PVT rings that are crystallized under various pressures and shear flows, the in situ structure formation for both molecular weights (iPP-1 and iPP-2) is studied by capturing WAXD and SAXS images upon shear flow in a Linkam shear cell in the BM26 beamline, part of the ESRF facility in Grenoble, France. For both the pure and compatibilized material, four different shear flows have been examined; as a benchmark experiment, the quiescent crystallization process is followed, while subsequently, shear flows at constant rates of 10, 50, and 90 s^{-1} are applied for 1 s. The crystallinity evolution as a function of time is presented in Figure 9 for both molecular weights at 5% of MAH-g-PP addition. Analogous to the previously discussed dilatometry results, with increasing flow strength, the crystallization kinetics are substantially enhanced. Although the final crystallinity of the compatibilized sample is slightly lower than the neat material under quiescent

https://doi.org/10.1021/acs.macromol.3c00603
Macromolecules 2023, 56, 5278−5289

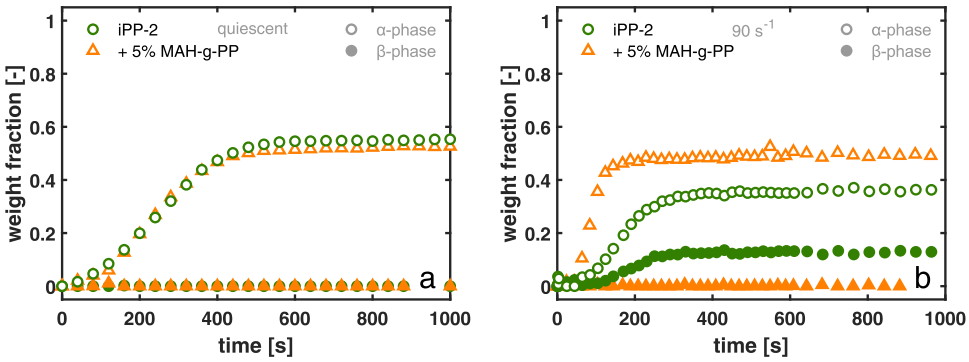

Figure 10. Phase composition of an iPP-2 sample after isothermal crystallization at 133 °C under (a) quiescent and (b) strong shear flow conditions. Whereas in the quiescent case, both the neat and compatibilized sample consist only of α-phase iPP, upon shear flow a large difference between the composition of the two samples can be observed.

conditions, this difference vanishes when a shear flow is applied. The apparent total crystallinity after shear flow is reduced by approximately 5−10% as compared to quiescent crystallization conditions. It should be highlighted once more that these experiments are combined SAXS/WAXD experiments, and because of the quasi-1D WAXD detector, the determination of absolute crystallinity is practically impossible. Hence, while the origin of this observed decrease in crystallinity may be a result of a change in morphology, a definitive argument cannot be given. The shear rates that are not presented here, i.e., 10 and 50 s^{-1}, can be found in the Supplementary Material. From the WAXD data, the phase composition can be calculated according to eq 6. The time evolution of the phase composition of iPP-2 is shown in Figure 10a under quiescent conditions where, as expected, the fraction of β-phase is equal to zero, i.e., no β-phase develops, for both the neat and compatibilized samples. After the application of shear (Figure 10b), the formation of β-iPP in the neat sample is considerable; due to the prealignment of molecular sections, small oriented α-phase crystals can form on which the β-modification is able to nucleate[27] and subsequently grow to a detectable amount. This mechanism of β-phase formation has been proposed in the literature by various authors and is in line with the results presented in Figure 10b, as first and increase in α-phase content is observed before the β-modification starts to form. The compatibilized sample on the other hand, shows faster kinetics (Figure 9b) but the formation of β-phase crystals is inherently absent.

While it may be impossible to directly translate these findings to a nucleation mechanism, as in these experiments merely bulk properties are assessed, the combination of the various techniques and protocols used in this work strongly suggests that the shear flow component is able to form the necessary oriented α-phase precursors only in the neat iPP material. Irrespective of the molecular weight and counter surface, e.g., steel in the dilatometer, glass in conventional microscopy, polyimide, and diamond in the Linkam shear cell, a strong bulk enhancement of the nucleation density is found when a slight amount of MAH-g-PP compatibilizer is added. It is therefore likely that the rapid space-filling by this vast amount of nuclei reduces the formation of the oriented α-phase from which the kinetically favored β-phase can grow. The practical implications thereof are already visualized by the optical micrographs presented in Figure 3, where the crystal formation around a single glass fiber is shown for both quiescent and shear flow conditions. Here, the before-mentioned effects, i.e., the strong acceleration of the crystallization kinetics, the vast amount of α-nuclei, and the disappearance of mesoscale lamellar orientation infer a strongly different crystalline microstructure at the interface of a fiber-reinforced polymer composite. The confirmation that the altered structure is a flow-induced effect from the bulk matrix implies that only due to local strain amplification it becomes apparent at the interphase, and that it is contrary to what is generally believed, not related to any adhesive interaction between the fiber and matrix. This has not only implications for the processing of these compatibilized polymer composites but also a pronounced effect on the resulting mechanical performance of such materials.

CONCLUSIONS

For a wide range of processing conditions, the effect of maleic anhydride compatibilization on the crystallization behavior of polypropylenes is assessed. Isothermal crystallization experiments are performed to quantify the crystal growth rate and nucleation density for both neat and compatibilized systems. Optical microscopy experiments show no dependence of the amount of MAH-g-PP compatibilizer nor the matrix molecular weight (of the composite and injection molding grade used) on the radial growth rate of spherulites. The nucleation density in the heterogeneous nucleation regime is found to be slightly larger for the blended systems, i.e., the MAH-g-PP compatibilizer mixed with neat iPP, as compared to both individual blend components. Due to the lower molecular weight of the modified polypropylene compatibilizer, a minute decrease in zero-shear viscosity of the blends is measured. However, given the rather large temperature dependence of all of the abovementioned parameters of polypropylene, the influence of maleic anhydride modification on the system can be considered negligible when the material is crystallized under quiescent conditions in a temperature gradient.

For industrially relevant conditions, however, a substantial effect of the incorporation of maleic anhydride is found. Using in situ density determination and X-ray scattering and diffraction experiments, the crystallization kinetics as well as the resulting microstructure and phase composition are measured. (I) For the various blends of MAH-g-PP with neat iPP, a strong acceleration of the crystallization kinetics is found, especially in the regime that is dominated by flow-enhanced nucleation. (II) Contrary to pure iPP systems, for these compatibilized materials, no oriented shish−kebab structures are observed at high shear rates. (III) Due to the

https://doi.org/10.1021/acs.macromol.3c00603
Macromolecules 2023, 56, 5278−5289

abundant nucleation of α-phase spherulites, the formation of the β-modification is suppressed, which intrinsically has a negative effect on the mechanical performance of iPP materials. The strong implications of these three effects for the structure formation upon the processing of iPP composites are highlighted by considering the crystallization around a glass fiber in shear flow conditions and may explain the contradictory results on the composite performance in the literature.

■ ASSOCIATED CONTENT

Supporting Information

The Supporting Information is available free of charge at https://pubs.acs.org/doi/10.1021/acs.macromol.3c00603.

Additional information on the characterization of the compounds (PDF)

■ AUTHOR INFORMATION

Corresponding Authors

Stan F. S. P. Looijmans − *Processing and Performance of Materials, Eindhoven University of Technology, 5600 MB Eindhoven, The Netherlands; Dutch Polymer Institute (DPI), 5600 AX Eindhoven, The Netherlands;* orcid.org/0000-0002-4148-8351; Email: S.F.S.P.Looijmans@tue.nl

Lambèrt C. A. van Breemen − *Processing and Performance of Materials, Eindhoven University of Technology, 5600 MB Eindhoven, The Netherlands;* orcid.org/0000-0002-0610-1908; Email: L.C.A.v.Breemen@tue.nl

Authors

Dario Cavallo − *Department of Chemistry and Industrial Chemistry, University of Genova, 16146 Genova, Italy;* orcid.org/0000-0002-3274-7067

Daniel Hermida Merino − *DUBBLE@ESRF, Netherlands Organization for Scientific Research (NWO), F38043 Grenoble, France; Departamento de Física Aplicada, CINBIO, Universidade de Vigo, E36310 Vigo, Spain*

Juan Carlos Martinez − *ALBA Synchrotron Light Source, 08290 Barcelona, Spain;* orcid.org/0000-0003-2411-5446

Patrick D. Anderson − *Processing and Performance of Materials, Eindhoven University of Technology, 5600 MB Eindhoven, The Netherlands*

Complete contact information is available at: https://pubs.acs.org/10.1021/acs.macromol.3c00603

Notes

The authors declare no competing financial interest.

■ ACKNOWLEDGMENTS

This research forms part of the research program of DPI, Project #815 PROFIT. Combined SAXS/WAXD single-shot experiments were performed at the BL11 NCD-SWEET beamline at ALBA Synchrotron with the collaboration of ALBA staff. In situ shear-cell experiments were performed on beamline BM26 at the European Synchrotron Radiation Facility (ESRF), Grenoble, France. The authors are grateful to all DUBBLE staff for providing assistance in using beamline BM26. In addition, the authors thank Bjorn Tuerlings from PTG/e for his assistance with compounding the materials, Jan−Hendrik Arndt (Fraunhofer) for performing the GPC-IR6 measurement on the compatibilizer, and Markus Gahleitner (Borealis) for his assistance in other GPC measurements.

■ REFERENCES

(1) Etcheverry, M.; Barbosa, S. E. Glass Fiber Reinforced Polypropylene Mechanical Properties Enhancement by Adhesion Improvement. *Materials* **2012**, *5*, 1084−1113.

(2) Luo, G.; Li, W.; Liang, W.; Liu, G.; Ma, Y.; Niu, Y.; Li, G. Coupling Effects of Glass Fiber Treatment and Matrix Modification on the Interfacial Microstructures and the Enhanced Mechanical Properties of Glass Fiber/Polypropylene Composites. *Composites, Part B* **2017**, *111*, 190−199.

(3) Uematsu, H.; Suzuki, Y.; Iemoto, Y.; Tanoue, S. Effect of Maleic Anhydride-Grafted Polypropylene on the Flow Orientation of Short Glass Fiber in Molten Polypropylene and on Tensile Properties of Composites. *Adv. Polym. Technol.* **2018**, *37*, 1755−1763.

(4) Bikiaris, D.; Matzinos, P.; Larena, A.; Flaris, V.; Panayiotou, C. Use of Silane Agents and Poly(Propylene-g-Maleic Anhydride) Copolymer as Adhesion Promoters in Glass Fiber/Polypropylene Composites. *J. Appl. Polym. Sci.* **2001**, *81*, 701−709.

(5) Boaen, N. K.; Hillmyer, M. A. Post-Polymerization Functionalization of Polyolefins. *Chem. Soc. Rev.* **2005**, *34*, 267−275.

(6) Gao, H.; Xie, Y.; Ou, R.; Wang, Q. Grafting Effects of Polypropylene/Polyethylene Blends with Maleic Anhydride on the Properties of the Resulting Wood−Plastic Composites. *Composites, Part A* **2012**, *43*, 150−157.

(7) Datta, S.; Lohse, D. J. Graft Copolymer Compatibilizers for Blends of Isotactic Polypropylene and Ethene-Propene Copolymers. 2. Functional Polymers Approach. *Macromolecules* **1993**, *26*, 2064−2076.

(8) Yang, H. S.; Kim, H. J.; Park, H. J.; Lee, B. J.; Hwang, T. S. Effect of Compatibilizing Agents on Rice-Husk Flour Reinforced Polypropylene Composites. *Compos. Struct.* **2007**, *77*, 45−55.

(9) Keener, T. J.; Stuart, R. K.; Brown, T. K. Maleated Coupling Agents for Natural Fibre Composites. *Composites, Part A* **2004**, *35*, 357−362.

(10) Kim, H. S.; Lee, B. H.; Choi, S. W.; Kim, S.; Kim, H. J. The Effect of Types of Maleic Anhydride-Grafted Polypropylene (MAPP) on the Interfacial Adhesion Properties of Bio-Flour-Filled Polypropylene Composites. *Composites, Part A* **2007**, *38*, 1473−1482.

(11) Gray, D. G. Transcrystallization of Polypropylene at Cellulose Nanocrystal Surfaces. *Cellulose* **2008**, *15*, 297−301.

(12) Nagy, B.; Varga, C. S.; Kontos, K.; Simon-Stöger, L. Remarkable Role of Experimental Olefin-Maleic-Anhydride Copolymer Based Compatibilizing Additives in Blends of Waste PET Bottles and Polyamide. *Waste Biomass Valorization* **2021**, *12*, 3035−3047.

(13) Panthapulakkal, S.; Sain, M. Injection-Molded Short Hemp Fiber/Glass Fiber-Reinforced Polypropylene Hybrid Composites−Mechanical, Water Absorption and Thermal Properties. *J. Appl. Polym. Sci.* **2007**, *103*, 2432−2441.

(14) Anandakumar, P.; Timmaraju, M. V.; Velmurugan, R. Development of Efficient Short/Continuous Fiber Thermoplastic Composite Automobile Suspension Upper Control Arm. *Mater. Today: Proc.* **2021**, *39*, 1187−1191.

(15) Heinen, W.; Rosenmöller, C. H.; Wenzel, C. B.; de Groot, H. J. M.; Lugtenburg, J.; Van Duin, M. 13C NMR Study of the Grafting of Maleic Anhydride onto Polyethene, Polypropene, and Ethene-Propene Copolymers. *Macromolecules* **1996**, *29*, 1151−1157.

(16) Gaylord, N. G.; Mishra, M. K. Nondegradative Reaction of Maleic Anhydride and Molten Polypropylene in the Presence of Peroxides. *J. Polym. Sci., Part B: Polym. Lett.* **1983**, *21*, 23−30.

(17) Severini, F.; Pegoraro, M.; Ricca, G.; Di Landro, L. New Additives in Glass Reinforced Polyolefins. *Makromol. Chem., Macromol. Symp.* **1989**, *28*, 217−229.

(18) Lazár, M.; Hrcková, L.; Fiedlerová, A.; Borsig, E.; Rätzsch, M.; Hesse, A. Functionalization of Isotactic Poly(Propylene) with Maleic Anhydride in the Solid Phase. *Angew. Makromol. Chem.* **1996**, *243*, 57−67.

(19) Minoura, Y.; Ueda, M.; Mizunuma, S.; Oba, M. The Reaction of Polypropylene with Maleic Anhydride. *J. Appl. Polym. Sci.* **1969**, *13*, 1625−1640.

(20) Shi, D.; Yang, J.; Yao, Z.; Wang, Y.; Huang, H.; Jing, W.; Yin, J.; Costa, G. Functionalization of Isotactic Polypropylene with Maleic Anhydride by Reactive Extrusion: Mechanism of Melt Grafting. *Polymer* **2001**, *42*, 5549−5557.
(21) Ni, Q. L.; Fan, J. Q.; Niu, H.; Dong, J. Y. Enhancement of Graft Yield and Control of Degradation during Polypropylene Maleation in the Presence of Polyfunctional Monomer. *J. Appl. Polym. Sci.* **2011**, *121*, 2512−2517.
(22) Diop, M. F.; Torkelson, J. M. Maleic Anhydride Functionalization of Polypropylene with Suppressed Molecular Weight Reduction via Solid-State Shear Pulverization. *Polymer* **2013**, *54*, 4143−4154.
(23) Zhang, M.; Colby, R. H.; Milner, S. T.; Chung, T. C. M.; Huang, T.; de Groot, W. Synthesis and Characterization of Maleic Anhydride Grafted Polypropylene with a Well-Defined Molecular Structure. *Macromolecules* **2013**, *46*, 4313−4323.
(24) Machado, A. V.; Covas, J. A.; Van Duin, M. Effect of Polyolefin Structure on Maleic Anhydride Grafting. *Polymer* **2001**, *42*, 3649−3655.
(25) Cho, K.; Li, F.; Choi, J. Crystallization and Melting Behavior of Polypropylene and Maleated Polypropylene Blends. *Polymer* **1999**, *40*, 1719−1729.
(26) Gray, D. G. "Transcrystallization" Induced by Mechanical Stress on a Polypropylene Melt. *J. Polym. Sci., Polym. Lett. Ed.* **1974**, *12*, 645−650.
(27) Varga, J.; Karger-Kocsis, J. Interfacial Morphologies in Carbon Fibre-Reinforced Polypropylene Microcomposites. *Polymer* **1995**, *36*, 4877−4881.
(28) Assouline, E.; Pohl, S.; Fulchiron, R.; Gérard, J. F.; Lustiger, A.; Wagner, H. D.; Marom, G. The Kinetics of α and β Transcrystallization in Fibre-Reinforced Polypropylene. *Polymer* **2000**, *41*, 7843−7854.
(29) Wang, K.; Guo, M.; Zhao, D.; Zhang, Q.; Du, R.; Fu, Q.; Dong, X.; Han, C. C. Facilitating Transcrystallization of Polypropylene/Glass Fiber Composites by Imposed Shear during Injection Molding. *Polymer* **2006**, *47*, 8374−8379.
(30) Zhang, S.; Minus, M. L.; Zhu, L.; Wong, C. P.; Kumar, S. Polymer Transcrystallinity Induced by Carbon Nanotubes. *Polymer* **2008**, *49*, 1356−1364.
(31) Li, H.; Yan, S. Surface-Induced Polymer Crystallization and the Resultant Structures and Morphologies. *Macromolecules* **2011**, *44*, 417−428.
(32) Ma, Z.; Balzano, L.; Van Erp, T. B.; Portale, G.; Peters, G. W. M. Short-Term Flow Induced Crystallization in Isotactic Polypropylene: How Short is Short? *Macromolecules* **2013**, *46*, 9249−9258.
(33) Looijmans, S. F. S. P.; Spanjaards, M. M. A.; Puskar, L.; Cavallo, D.; Anderson, P. D.; Van Breemen, L. C. A. Synergy of Fiber Surface Chemistry and Flow: Multi-Phase Transcrystallization in Fiber-Reinforced Thermoplastics. *Polymers* **2022**, *14*, 4850.
(34) Fu, X.; He, B.; Chen, X. Effects of Compatibilizers on Mechanical Properties of Long Glass Fiber-Reinforced Polypropylene. *J. Reinf. Plast. Compos.* **2010**, *29*, 936−949.
(35) Zhang, K.; Guo, Q.; Zhang, D.; Guo, J. Mechanical Properties and Morphology of Polypropylene/Polypropylene-g-Maleic Anhydride/Long Glass Fiber Composites. *J. Macromol. Sci., Part B: Phys.* **2015**, *54*, 286−294.
(36) Tjong, S. C.; Xu, S. A.; Li, R. K. Y.; Mai, Y. W. Mechanical Behavior and Fracture Toughness Evaluation of Maleic Anhydride Compatibilized Short Glass Fiber/SEBS/Polypropylene Hybrid Composites. *Compos. Sci. Technol.* **2002**, *62*, 831−840.
(37) Quan, H.; Li, Z. M.; Yang, M. B.; Huang, R. On Transcrystallinity in Semi-Crystalline Polymer Composites. *Compos. Sci. Technol.* **2005**, *65*, 999−1021.
(38) Chen, E. J. H.; Hsiao, B. S. The Effects of Transcrystalline Interphase in Advanced Polymer Composites. *Polym. Eng. Sci.* **1992**, *32*, 280−286.
(39) Sorrentino, L.; Simeoli, G.; Iannace, S.; Russo, P. Mechanical Performance Optimization through Interface Strength Gradation in PP/Glass Fibre Reinforced Composites. *Composites, Part B* **2015**, *76*, 201−208.
(40) Ning, N.; Fu, S.; Zhang, W.; Chen, F.; Wang, K.; Deng, H.; Zhang, Q.; Fu, Q. Realizing the Enhancement of Interfacial Interaction in Semicrystalline Polymer/Filler Composites via Interfacial Crystallization. *Prog. Polym. Sci.* **2012**, *37*, 1425−1455.
(41) Guo, M.; Yang, H.; Tan, H.; Wang, C.; Zhang, Q.; Du, R.; Fu, Q. Shear Enhanced Fiber Orientation and Adhesion in PP/Glass Fiber Composites. *Macromol. Mater. Eng.* **2006**, *291*, 239−246.
(42) Xie, M.; Chang, B.; Liu, H.; Dai, K.; Zheng, G.; Liu, C.; Shen, C.; Chen, J. Enhanced β-Crystal Formation of Isotactic Polypropylene under the Combined Effects of Acid-Corroded Glass Fiber and Preshear. *Polym. Compos.* **2013**, *34*, 1250−1260.
(43) Sheng, Q.; Zhang, Y.; Xia, C.; Mi, D.; Xu, X.; Wang, T.; Zhang, J.; New, A. Insight into the Effect of β Modification on the Mechanical Properties of iPP: The Role of Crystalline Morphology. *Mater. Des.* **2016**, *95*, 247−255.
(44) Gati, A.; Wagner, H. D. Stress Transfer Efficiency in Semicrystalline-Based Composites Comprising Transcrystalline Interlayers. *Macromolecules* **1997**, *30*, 3933−3935.
(45) Stern, T.; Teishev, A.; Marom, G. Composites of Polyethylene Reinforced with Chopped Polyethylene Fibers: Effect of Transcrystalline Interphase. *Compos. Sci. Technol.* **1997**, *57*, 1009−1015.
(46) Li, W.; Chen, W.; Tang, L.; Jiang, Z.; Huang, P. A General Strength Model for Fiber Bundle Composites under Transverse Tension or Interlaminar Shear. *Composites, Part A* **2019**, *121*, 45−55.
(47) Thomason, J. L.; Yang, L. Temperature Dependence of the Interfacial Shear Strength in Glass-Fibre Polypropylene Composites. *Compos. Sci. Technol.* **2011**, *71*, 1600−1605.
(48) Grosso, G.; Troisi, E. M.; Jaensson, N. O.; Peters, G. W. M.; Anderson, P. D. Modelling Flow Induced Crystallization of iPP: Multiple Crystal Phases and Morphologies. *Polymer* **2019**, *182*, No. 121806.
(49) Thomason, J. L. Glass Fibre Sizing: A Review. *Composites, Part A* **2019**, *127*, No. 105619.
(50) Brückner, S.; Meille, S. V.; Petraccone, V.; Pirozzi, B. Polymorphism in Isotactic Polypropylene. *Prog. Polym. Sci.* **1991**, *16*, 361−404.
(51) De Rosa, C.; Auriemma, F.; Di Girolamo, R.; De Ballesteros, O. R.; Pepe, M.; Tarallo, O.; Malafronte, A. Morphology and Mechanical Properties of the Mesomorphic Form of Isotactic Polypropylene in Stereodefective Polypropylene. *Macromolecules* **2013**, *46*, 5202−5214.
(52) Meille, S. V.; Brückner, S. Non-Parallel Chains in Crystalline γ-Isotactic Polypropylene. *Nature* **1989**, *340*, 455−457.
(53) Mezghani, K.; Phillips, P. J. The γ-Phase of High Molecular Weight Isotactic Polypropylene. II: The Morphology of the γ-Form Crystallized at 200 MPa. *Polymer* **1997**, *38*, 5725−5733.
(54) Meille, S. V.; Ferro, D. R.; Brückner, S.; Lovinger, A. J.; Padden, F. J. Structure of β-Isotactic Polypropylene: A Long-Standing Structural Puzzle. *Macromolecules* **1994**, *27*, 2615−2622.
(55) Varga, J. β-Modification of Isotactic Polypropylene: Preparation, Structure, Processing, Properties, and Application. *J. Macromol. Sci., Part B* **2002**, *41*, 1121−1171.
(56) Lovinger, A. J.; Chua, J. O.; Gryte, C. C. Studies on the α and β Forms of Isotactic Polypropylene by Crystallization in a Temperature Gradient. *J. Polym. Sci., Polym. Phys. Ed.* **1977**, *15*, 641−656.
(57) Tang, X. G.; Yang, W.; Shan, G. F.; Yang, B.; Xie, B. H.; Yang, M. B.; Hou, M. Effect of Temperature Gradient on the Development of β Phase Polypropylene in Dynamically Vulcanized PP/EPDM Blends. *Colloid Polym. Sci.* **2009**, *287*, 1237−1242.
(58) Varga, J.; Karger-Kocsis, J. Rules of Supermolecular Structure Formation in Sheared Isotactic Polypropylene Melts. *J. Polym. Sci., Part B: Polym. Phys.* **1996**, *34*, 657−670.
(59) Somani, R. H.; Hsiao, B. S.; Nogales, A.; Fruitwala, H.; Srinivas, S.; Tsou, A. H. Structure Development during Shear Flow Induced Crystallization of i-PP: In Situ Wide-Angle X-Ray Diffraction Study. *Macromolecules* **2001**, *34*, 5902−5909.

https://doi.org/10.1021/acs.macromol.3c00603
Macromolecules 2023, 56, 5278−5289

(60) Caelers, H. J. M.; Parodi, E.; Cavallo, D.; Peters, G. W. M.; Govaert, L. E. Deformation and Failure Kinetics of iPP Polymorphs. *J. Polym. Sci., Part B: Polym. Phys.* **2017**, *55*, 729−747.
(61) Varga, J.; Mudra, I.; Ehrenstein, G. W. Highly Active Thermally Stable β-Nucleating Agents for Isotactic Polypropylene. *J. Appl. Polym. Sci.* **1999**, *74*, 2357−2368.
(62) Van der Beek, M. H. E.; Peters, G. W. M.; Meijer, H. E. H. Influence of Shear Flow on the Specific Volume and the Crystalline Morphology of Isotactic Polypropylene. *Macromolecules* **2006**, *39*, 1805−1814.
(63) Housmans, J. W.; Steenbakkers, R. J. A.; Roozemond, P. C.; Peters, G. W. M.; Meijer, H. E. H. Saturation of Pointlike Nuclei and the Transition to Oriented Structures in Flow-Induced Crystallization of Isotactic Polypropylene. *Macromolecules* **2009**, *42*, 5728−5740.
(64) De Santis, F.; Pantani, R. Nucleation Density and Growth Rate of Polypropylene Measured by Calorimetric Experiments. *J. Therm. Anal. Calorim.* **2013**, *112*, 1481−1488.
(65) Forstner, R.; Peters, G. W. M.; Meijer, H. E. H. A Novel Dilatometer for PVT Measurements of Polymers at High Cooling- and Shear Rates. *Int. Polym. Process.* **2009**, *24*, 114−121.
(66) Housmans, J. W.; Balzano, L.; Adinolfi, M.; Peters, G. W. M.; Meijer, H. E. H. Dilatometry: A Tool to Measure the Influence of Cooling Rate and Pressure on the Phase Behavior of Nucleated Polypropylene. *Macromol. Mater. Eng.* **2009**, *294*, 231−243.
(67) He, J.; Zoller, P. Crystallization of Polypropylene, Nylon-66 and Poly(Ethylene Terephthalate) at Pressures to 200 MPa: Kinetics and Characterization of Products. *J. Polym. Sci., Part B: Polym. Phys.* **1994**, *32*, 1049−1067.
(68) Van Erp, T. B.; Balzano, L.; Spoelstra, A. B.; Govaert, L. E.; Peters, G. W. M. Quantification of Non-Isothermal, Multi-Phase Crystallization of Isotactic Polypropylene: The Influence of Shear and Pressure. *Polymer* **2012**, *53*, 5896−5908.
(69) Cardinaels, R.; Van Puyvelde, P.; Moldenaers, P. Evaluation and Comparison of Routes to Obtain Pressure Coefficients from High-Pressure Capillary Rheometry Data. *Rheol. Acta* **2007**, *46*, 495−505.
(70) Kadijk, S. E.; Van den Brule, B. H. A. A. On the Pressure Dependency of the Viscosity of Molten Polymers. *Polym. Eng. Sci.* **1994**, *34*, 1535−1546.
(71) González Fernández, J.; Colldelram, C.; Ferrer, S.; Fontserè Recuenco, A.; Gevorgyan, A.; González, N.; Jover-Manas, G.; Kamma-Lorger, C.; Llonch, M.; Malfois, M.; Juan Martínez Guil; Nikitin, Y.; Pena, G.; Ribó, L.; Sics, I.; Solano, E.; Villanueva, J. In *NCD-SWEET Beamline Upgrade, Proceedings of the 10th Mechanical Engineering Design Synchrotron Radiation Equipment Instruments, Paris, Franch*, 2018; pp 374−376.
(72) Nikitenko, S.; Beale, A. M.; Van der Eerden, A. M. J.; Jacques, S. D. M.; Leynaud, O.; O'Brien, M. G.; Detollenaere, D.; Kaptein, R.; Weckhuysen, B. M.; Bras, W. Implementation of a Combined SAXS/WAXS/QEXAFS Set-Up for Time-Resolved In-Situ Experiments. *J. Synchrotron Radiat.* **2008**, *15*, 632−640.
(73) Hammersley, A. P.; Svensson, S. O.; Hanfland, M.; Fitch, A. N.; Häusermann, D. Two-Dimensional Detector Software: From Real Detector to Idealised Image or Two-Theta Scan. *High Pressure Research* **1996**, *14*, 235−248.
(74) Hammersley, A. P. *FIT2D: An Introduction and Overview*, 1997.
(75) Hammersley, A. P. *FIT2D V9.129 Reference Manual V3.1*, 1998.
(76) Caelers, H. J. M.; Troisi, E. M.; Govaert, L. E.; Peters, G. W. M. Deformation-Induced Phase Transitions in iPP Polymorphs. *Polymers* **2017**, *9*, 547.
(77) Isasi, J. R.; Mandelkern, L.; Galante, M. J.; Alamo, R. G. The Degree of Crystallinity of Monoclinic Isotactic Poly(Propylene). *J. Polym. Sci., Part B: Polym. Phys.* **1999**, *37*, 323−334.
(78) Quynn, R. G.; Riley, J. L.; Young, D. A.; Noether, H. D. Density, Crystallinity, and Heptane Insolubility in Isotactic Polypropylene. *J. Appl. Polym. Sci.* **1959**, *2*, 166−173.
(79) Kawasumi, M.; Hasegawa, N.; Kato, M.; Usuki, A.; Okada, A. Preparation and Mechanical Properties of Polypropylene-Clay Hybrids. *Macromolecules* **1997**, *30*, 6333−6338.
(80) Van Drongelen, M.; Van Erp, T. B.; Peters, G. W. M. Quantification of Non-Isothermal, Multi-Phase Crystallization of Isotactic Polypropylene: The Influence of Cooling Rate and Pressure. *Polymer* **2012**, *53*, 4758−4769.
(81) Lauritzen, J. I.; Hoffman, J. D. Extension of Theory of Growth of Chain-Folded Polymer Crystals to Large Undercoolings. *J. Appl. Phys.* **1973**, *44*, 4340−4352.
(82) Avrami, M. Kinetics of Phase Change. I General Theory. *J. Chem. Phys.* **1939**, *7*, 1103−1112.
(83) Avrami, M. Kinetics of Phase Change. II Transformation-Time Relations for Random Distribution of Nuclei. *J. Chem. Phys.* **1940**, *8*, 212−224.
(84) Lamberti, G. Isotactic Polypropylene Crystallization: Analysis and Modeling. *Eur. Polym. J.* **2011**, *47*, 1097−1112.
(85) Schneider, W.; Köppl, A.; Berger, J. Non−Isothermal Crystallization of Polymers. *Int. Polym. Process.* **1988**, *2*, 151−154.
(86) Caelers, H. J. M.; de Cock, A.; Looijmans, S. F. S. P.; Kleppinger, R.; Troisi, E. M.; Van Drongelen, M.; Peters, G. W. M. An Experimentally Validated Model for Quiescent Multiphase Primary and Secondary Crystallization Phenomena in PP with Low Content of Ethylene Comonomer. *Polymer* **2022**, *253*, No. 124901.
(87) Lorenzo, A. T.; Arnal, M. L.; Albuerne, J.; Müller, A. J. DSC Isothermal Polymer Crystallization Kinetics Measurements and the Use of the Avrami Equation to Fit the Data: Guidelines to Avoid Common Problems. *Polym. Test.* **2007**, *26*, 222−231.
(88) Pérez-Camargo, R. A.; Liu, G. M.; Wang, D. J.; Müller, A. J. Experimental and Data Fitting Guidelines for the Determination of Polymer Crystallization Kinetics. *Chin. J. Polym. Sci.* **2022**, *40*, 658−691.

https://doi.org/10.1021/acs.macromol.3c00603
Macromolecules 2023, 56, 5278−5289